Numerical Simulation Model for Cryogenic Pump Cavitation

Naoki TANI
Department of Aeronautics and Astronautics, University of Tokyo
7-3-1 Hongo Bunkyo-ku Tokyo 113-8656, Japan
tani@thermo.t.u-tokyo.ac.jp

Toshio NAGASHIMA
Department of Aeronautics and Astronautics, University of Tokyo
7-3-1 Hongo Bunkyo-ku Tokyo 113-8656, Japan
tnaga@mail.ecc.u-tokyo.ac.jp

Keywords: Cavitation, Cryogenic, Pump, CFD

Abstract

In the development of rocket turbo-pump, cavitation at the inducer is one of the major problems. Cryogenic fluids are commonly used for rocket propellant, therefore, thermodynamic effect becomes noticeable compared to conventional water cavitation. In the present study, a numerical simulation method for cryogenic cavitation is proposed, which reveals the difference between cryogenic and water cavitation.

Introduction

Recent high performance rocket engine requires extremely high combustion chamber pressure, therefore, turbo pumps become operated at very high rotating speed, so that cavitation at the inducer becomes a serious problem. Since cavitation induces unstable oscillation and steep efficiency drop, it has been a major problem for marine propellers and pumps. In rocket turbo pumps, since working fluid is cryogenic like liquid oxygen and liquid hydrogen, the temperature in cavitation region drops slightly due to latent heat absorption, as a result, cavitation performance becomes improved in cryogenic fluid. This is called 'thermodynamic effect' of cryogenic cavitation. However, even in recent days, experiments and calculations upon cryogenic cavitation are relatively few.

In conventional water cavitation calculation, energy equation is usually neglected since the thermal capacity of liquid is extremely large compared to that of gas. However, in cryogenic fluid, temperature change occurs due to latent heat absorption, as a result, energy equation must be solved.

In the present study, a numerical simulation model for cryogenic cavitation simulation is presented, which reveals the difference between cryogenic and conventional water cavitation.

Governing Equations

Flow Equations

Governing equations of two dimensional cavitating flow are written as follows.

$$\frac{\partial}{\partial t}\begin{bmatrix}\rho\\ \rho u\\ \rho v\\ \rho e\end{bmatrix}+\frac{\partial}{\partial x}\cdot\begin{bmatrix}\rho u\\ P+\rho u^2\\ \rho uv\\ (\rho e+P)u\end{bmatrix}+\frac{\partial}{\partial y}\cdot\begin{bmatrix}\rho v\\ \rho uv\\ P+\rho v^2\\ (\rho e+P)v\end{bmatrix}=\begin{bmatrix}0\\ 0\\ 0\\ 0\end{bmatrix} \quad (1)$$

where, ρ, u, v, e and P are density, x and y component of velocity, specific total energy and pressure, respectively. Usually, energy equation is neglected in conventional water cavitation cases, however, this equation must be considered in thermo-sensitive cryogenic fluid. The formulation takes the same as the single-phase Euler equations, however, density and energy are modified to the following averaged form of gas and liquid.

$$\rho=\alpha\cdot\rho_g+(1-\alpha)\cdot\rho_l \quad (2)$$

$$e=[\chi C_{vg}+(1-\chi)C_{vl}]\cdot T+\tfrac{1}{2}|\mathbf{u}|^2+[\chi E_g+(1-\chi)E_l] \quad (3)$$

Here, α, χ, Cv, E, T and **u** are gas phase volume fraction (void fraction), mass fraction (quality), specific heat at constant volume, internal energy at reference temperature, temperature and velocity vector, respectively, and subscript g and l mean gas (vapor) and liquid phase. The third term of energy equation (3) indicates latent heat term, and difference of E_l and E_g represents latent heat at vaporizations.

State equation is also modified to two-phase form. Presently, a two-phase averaged state equation derived by Okuda et al.[1] is applied.

$$\rho=\frac{P+P_{ct}}{K_{ct}(T+T_{ct})}(1-\alpha)+\frac{P}{R_{ct}T}\alpha \quad (4)$$

Where, P_{ct}, K_{ct}, T_{ct} and R_{ct} are pressure constant, liquid constant, temperature constant and gas constant, respectively. In order to obtain α, cavitation model, which is explained in the next section, is required.

Cavitation Model

In the present paper, Bubble Two-phase Flow (BTF) model[2] was applied as cavitation model, since it can handle non-linear bubble dynamics. This model assumes cavitation as a cluster of tiny spherical bubbles, and these bubble motions are governed by Reyleigh-Plesset equation.

$$R\frac{D^2R}{Dt^2}+\frac{3}{2}\left(\frac{DR}{Dt}\right)^2=\frac{P_{sat}-P}{\rho_l} \quad (5)$$

where, R is bubble radius and subscript 'sat' indicates saturation condition. D/Dt represents as follows.

$$\frac{D}{Dt}=\frac{d}{dt}+u\frac{\partial}{\partial x}+v\frac{\partial}{\partial v} \quad (6)$$

Equation (5) contains 2nd order time derivative, therefore, time marching scheme can not be adopted. In order to overcome this difficulty, equation (5) is separated into two equations.

$$\frac{DR}{Dt}=S \quad (7)$$

$$\frac{DS}{Dt}=\frac{1}{R}\left(\frac{P_{sat}-P}{\rho_l}-\frac{3}{2}S^2\right) \quad (8)$$

where, S is a bubble wall velocity. According to these equations, void fraction α can be derived as follows.

$$\alpha=\frac{4}{3}\pi R^3 N \quad (9)$$

where, N represents bubble number density per unit volume, and in the present calculation, this value was set to 1.6×10^9 [3].

Solution Procedure

One of the key features of cavitating flow is a mixture of compressible and incompressible fluid. Fig. 1 shows a sound speed change against void fraction, and this plot indicates that the sound speed of two-phase flow region becomes very low, as a result, cavitating region easily becomes supersonic. In order to handle such a compressible and incompressible mixture flow, TCUP method[4] was applied, which is one of the high-resolution procedure to handle high speed and temperature sensitive two-phase flow. TCUP method divides governing equations into three steps, advection, acoustic and non-advection step, which is shown in fig.2. To solve bubble equation (7) and (8), in order to simplify solution procedure, equations are expressed by using quality χ.

$$\frac{D\chi}{Dt}=\beta \quad (10)$$

$$\frac{D\beta}{Dt}=\frac{1}{\chi}\left[-\frac{3}{2}\beta^2+3\frac{P_{sat}-P}{\rho_l}\cdot\left(\frac{4\pi\rho_g N}{3\rho}\right)^{2/3}\right] \quad (11)$$

where, β denotes mass phase change rate. These equations are also divided into three steps.

- Advection Step

$$\frac{D}{Dt}\left(\frac{\rho}{\rho_g}\chi\right)=0 \quad (12)$$

$$\frac{D\beta}{Dt}=0 \quad (13)$$

- Acoustic Step

$$\frac{d\chi}{dt}=0 \quad (14)$$

$$\frac{d\beta}{dt}=0 \quad (15)$$

- Non-Advection Step

$$\frac{d\chi}{dt}=\beta \quad (16)$$

$$\frac{d\beta}{dt}=\frac{1}{\chi}\left[-\frac{3}{2}\beta^2+3\frac{P_{sat}-P}{\rho_l}\cdot\left(\frac{4\pi\rho_g N}{3\rho}\right)^{2/3}\right] \quad (17)$$

These procedures are also described in fig.2. In advection step, in order to improve conservation, minor modification was applied ($\frac{\rho}{\rho_g}\chi$ equals to α).

In solving these equations, the time scale of bubble motion is very small compared to that of main flow. Therefore, inner iteration method is applied to non-advection step bubble motion procedure, that is, time step of bubble motion procedure makes several times smaller than that of main flow, and iteration is carried out until catch up with the main flow time step.

Appling the above procedure, calculation advances very efficiently.

Single Bubble Motion

Firstly, validation of single bubble motion is carried out, in which only equations (10) and (11) are solved, and ambient pressure and temperature are set to be unchanged by bubble motion. Schematic view of the corresponding calculation region is shown in fig. 3. Single bubble is convected by constant velocity U_b (5m/s) and ambient pressure distribution makes bubble motion. From Lagrangian view, elapsed time of bubble becomes as follows.

$$t=\frac{x}{U_b} \quad (16)$$

In Fig. 4, bubble radius history is shown at bubble collapse. Ambient pressure is initially set equal to saturation pressure ($P=P_{sat}$) and, at $t=1.0\times10^{-4}$, it is multiplied to 1.5 times larger ($P=1.5P_{sat}$). Collapsing time t_{dist} is given by following equation.

$$t_{dest}=0.915R_0\sqrt{\frac{\rho_l}{P-P_{sat}}} \quad (16)$$

where, R_0 means initial radius. According to fig.4, good agreement can be observed between moving bubble and theoretical value.

Validation of bubble growth is also compared in fig. 5. In this calculation, ambient pressure is also set to saturation pressure at initial condition, and, at $t=3.0\times10^{-4}$, pressure is decreased to 70% saturation pressure. Theoretical growth speed $\left.\frac{dR}{dt}\right|_{grow}$ can be given as following.

$$\left.\frac{dR}{dt}\right|_{grow}=\sqrt{\frac{2}{3}\frac{P_{sat}-P}{\rho_l}} \quad (17)$$

Comparison reveals good agreement in bubble generation, too.

Simplified Reyleigh-Plesset equation is often used in cavitation calculation[5].

$$\frac{dR}{dt} = \frac{P_{sat} - P}{|P_{sat} - P|}\sqrt{\frac{2}{3}\frac{|P_{sat} - P|}{\rho_l}} \qquad (18)$$

This equation is derived by neglecting higher order term of equation (5). Fig. 6 shows the comparison of bubble radius derived from simplified and exact Reyleigh-Plesset equation. Ambient pressure oscillates randomly and at $t = 1.2\times10^{-3}$, ambient pressure becomes equal to the saturation pressure. This result reveals that bubble radius from exact equation continues to grow, on the contrary, bubble radius growth from simplified form remains constant radius. This comparison indicates that the simplified form may estimate cavitation smaller.

In summary, moving bubble can be properly treated by present method, and this result indicates that BTF model can be applicable to TCUP method.

Thermodynamic Effect

In order to compare thermodynamic effect, calculations around two-dimensional NACA0015 airfoil were carried out. Uniform flow velocity is set at 5m/s, while working fluids are 290K water and 78K liquid nitrogen (LN2). Ambient pressure is set by using the cavitation number σ.

$$\sigma = \frac{P_{ref} - P_{sat}}{\frac{1}{2}\rho_{ref} u_{ref}^2} \qquad (19)$$

where, subscript ref means reference value, and in this calculation, reference point is set at the inlet value. Presently, σ is set at 1.5 in both fluids. Computational grid is shown in fig.7, and grid points are in total 12000 points. Angle of attack is set to 8 degrees.

Cavitation shape comparison is shown in fig.8, and this comparison reveals that cavitation shape is completely different from each other. In fig.9, pressure coefficient distribution at airfoil surface is shown. The definition of Pressure coefficient Cp is,

$$C_p = \frac{P - P_{ref}}{\frac{1}{2}\rho_{ref} u_{ref}^2} \qquad (20)$$

This pressure comparison reveals that liquid nitrogen pressure inside the cavitation becomes lower than that of water. This difference is derived from the fluid property. Temperature decrease ΔT_{lat} due to latent heat absorption per unit volume is derived as follow,

$$\Delta T = \frac{L}{\rho_l / \rho_g \, C_{pl}} \frac{\alpha}{1-\alpha} \qquad (21)$$

where, L and Cpl mean latent heat and specific heat at constant pressure of liquid phase, respectively. Assuming that pressure in the cavity is maintained at the saturated condition, pressure decrease ΔP can be estimated.

$$\Delta P = \left.\frac{dP}{dT}\right|_{sat} \Delta T = \frac{L}{\rho_l / \rho_g \, C_{pl}} \frac{\alpha}{1-\alpha} \left.\frac{dP}{dT}\right|_{sat} \qquad (22)$$

In fig.10, ΔP value against void fraction is shown, and pressure depression of liquid nitrogen becomes larger than that of water. Table 1 shows the comparison of each physical values of equation (21), and this table indicates that pressure depression difference is caused by density ratio and $\left.\frac{dP}{dT}\right|_{sat}$ value.

Table 1 Thermodynamic properties of water and liquid nitrogen

	Water	LN2
L[J/kg]	2461×10^3	199.1×10^3
ρ_l/ρ_g [-]	69375.	181.3
C_{pl} [J/kg/K]	4184.	2060.
$\left.\frac{dP}{dT}\right\|_{sat}$	1.27×10^2	1.16×10^4
$\frac{L}{\rho_l/\rho_g \, C_{pl}} \cdot \left.\frac{dP}{dT}\right\|_{sat}$	1.08	6183.

In order to investigate the influence of the thermodynamic effect upon overall performance, lift coefficient C_L change against σ was examined in fig.11. Definition of C_L is,

$$C_L = \frac{F_L}{\frac{1}{2}\rho_{ref} u_{ref}^2} \qquad (23)$$

where, F_L means lift force. The plots clearly indicate that the lift coefficient of liquid nitrogen improved at low σ. Pressure coefficient distribution at σ=0.5 in fig.12 indicates that low pressure region at the cavitation in liquid nitrogen becomes larger, as a result, total lift is maintained high compared to water at low cavitation number. This tendency qualitatively agrees with the finding of inducer test[6].

Conclusions

In the present study, numerical simulation model to handle cryogenic cavitating flow was proposed, and revealed the difference between cryogenic and conventional cavitation. In summary, following points were concluded.

- BTF cavitation model was validated against single bubble motion, and it can be properly coupled to TCUP method.
- In cryogenic cavitation calculation, proper treatment of energy equation and latent heat is required
- Improvement of lift coefficient at low cavitation number in cryogenic fluid was observed by numerical simulation.

Acknowledgement

The authors were supported through the 21st Century COE Program, "Mechanical System Innovation," by the Ministry of Education, Culture, Sports Science and Technology.

References

1) Okuda, K, Ikohagi, T.: Numerical Simulation of Collapsing Behavior of Bubble Clouds, *Trans. JSME series(B)*, **62**, 1996, pp.3792-3793
2) Kubota, A., Kato, H. and Yamaguchi, H.: A New Modelling of Cavitation Flows –A Numerical Study of Unsteady Cavitation on Hydrofoil Section, *J. Fluid. Mech.*, **240**, 1992, pp.59-96
3) Wang, Y.: Effect of Nuclei Size Distribution on the Dynamics of a Spherical Clouds of Cavitation Bubbles, *J. Fluid Eng.*, **121**, 1999, pp.881-886
4) Himeno, T. Watanabe, T. and Konno, A.: Numerical Analysis for Propellant Management in Liquid Rocket Tank, *AIAA2001-3822*, 2001
5) Bernstern, G.S., Kjeldsen, M. and Arndt, R.E.A.: Numerical Modeling of Sheet ant Tip Vortex Cavitation with FLUENT5, *Proceedings of 4th International Symposium on Cavitation*, session B5-006, 2001
6) Yamada, H., Watanabe, Y. and Hirata, K.: An Experimental Study of a Small High-Speed LH2 Pump for Rocket, NAL TR-1131

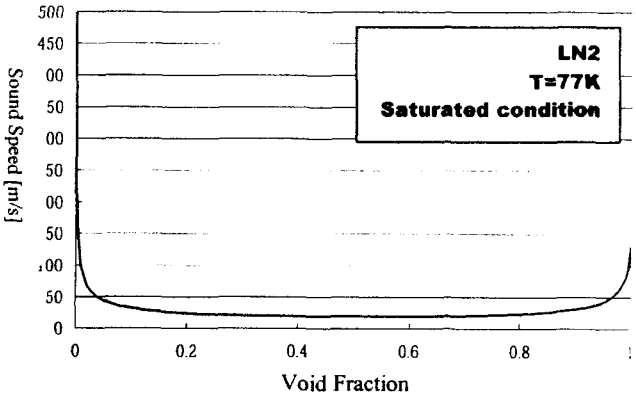

Fig.1 Sound speed of two phase flow

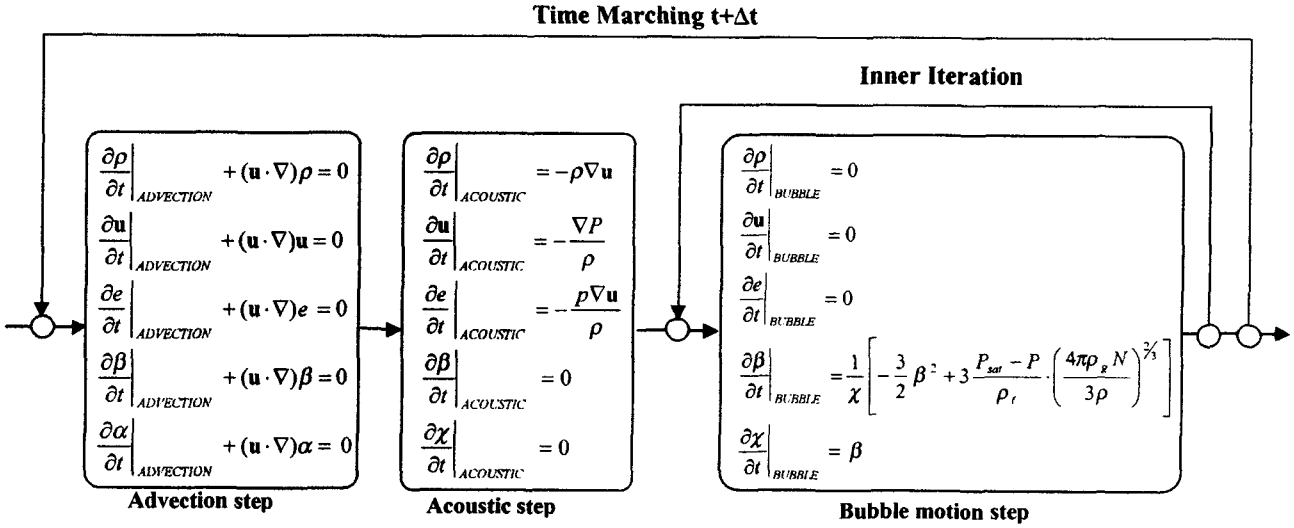

Fig. 2 Solution procedure diagram

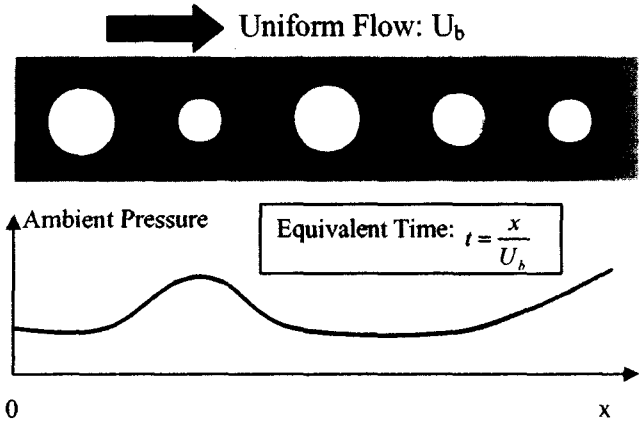

Fig. 3 Schematic view of single bubble calculation validation

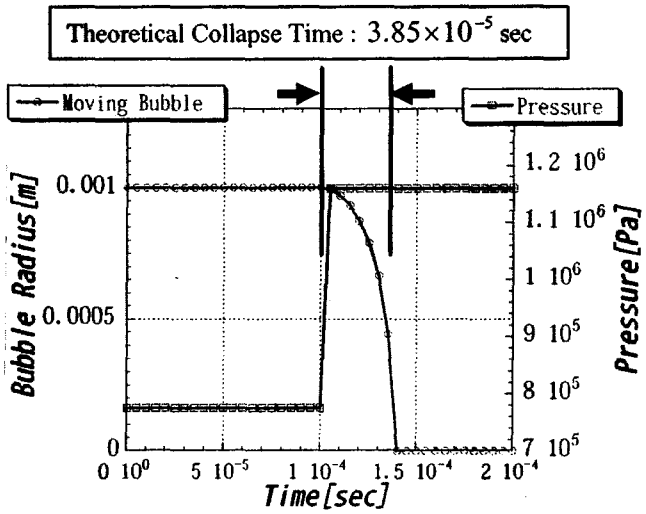

Fig. 4 Single bubble radius history at collapse

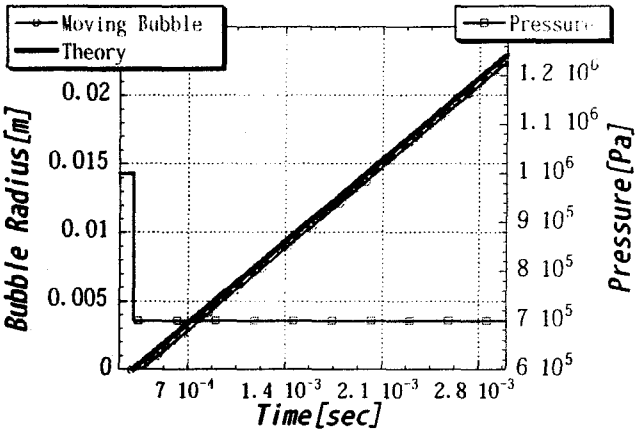

Fig. 5 Single bubble radius history at generation

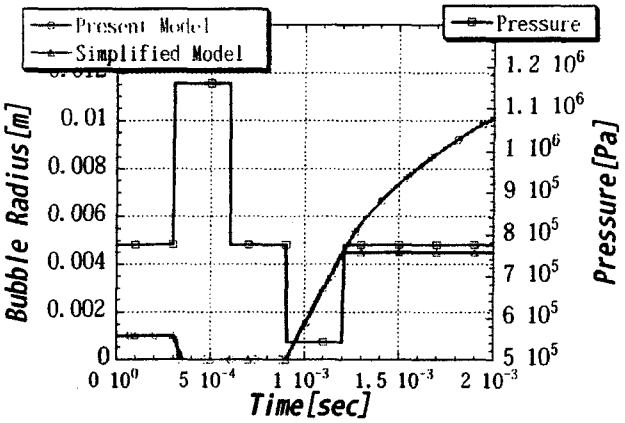

Fig. 6 Bubble radius history comparison between full and simplified bubble equation

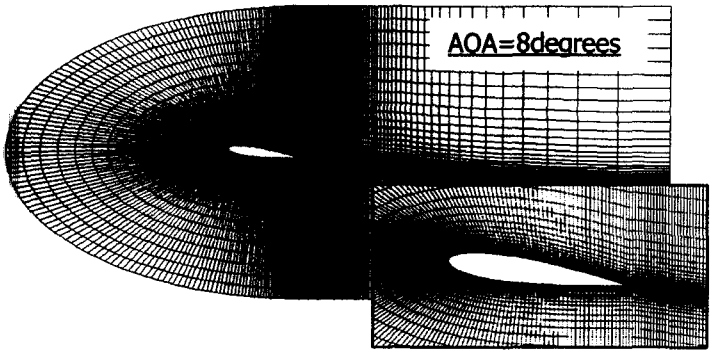

Fig. 7 Computational gird of NACA0015 profile

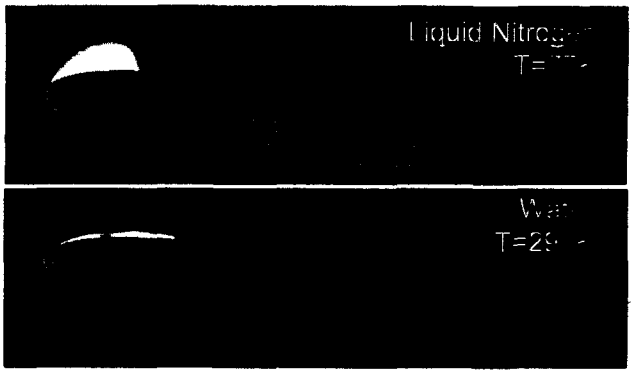

Fig. 8 Cavitation pattern of liquid nitrogen and water

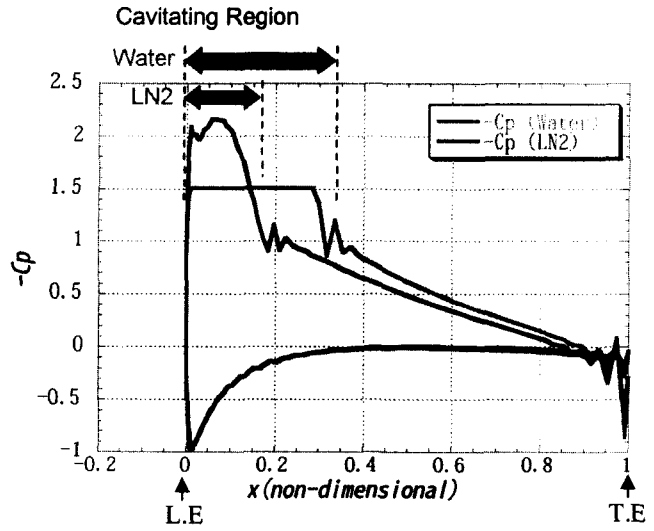

Fig. 9 Pressure coefficient distribution on airfoil surface σ=1.5

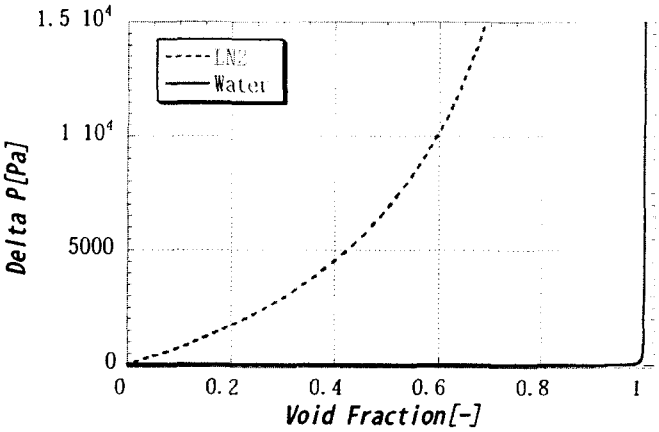

Fig. 10 Pressure decrease against void fraction

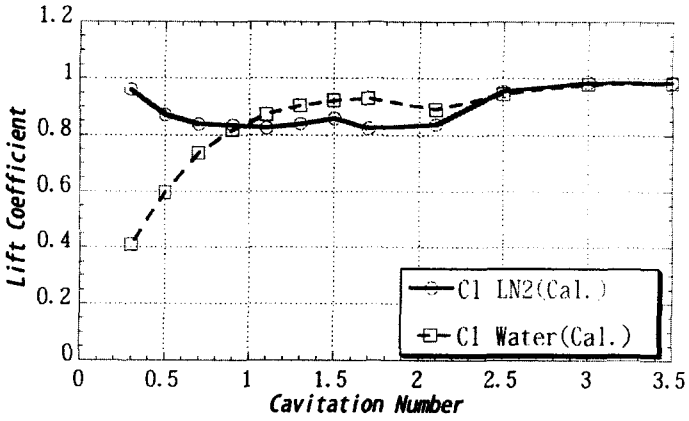

Fig. 11 Lift coefficient against σ

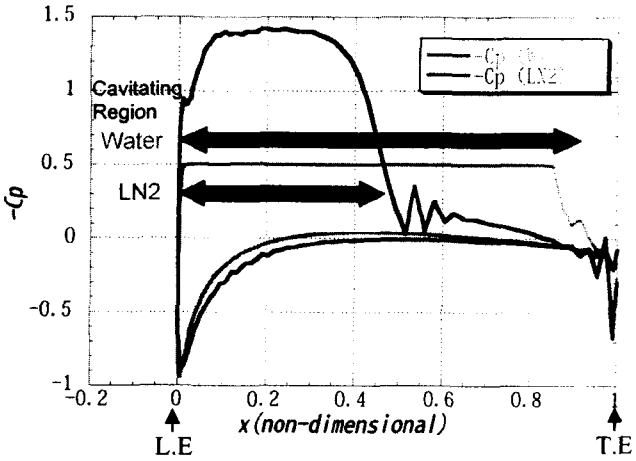

Fig. 12 Pressure coefficient distribution on airfoil surface σ=0.5